

DEVELOPMENT OF A PRECISION PEPPER-POT EMITTANCE METER

G. Hahn*, Pohang Accelerator Laboratory (PAL), 37673 Pohang, South Korea
J.G. Hwang, Helmholtz-Zentrum Berlin (HZB), 12489 Berlin, Germany

Abstract

A fast single-shot emittance measurement device, a pepper-pot emittance meter, was developed to utilize it at the heavy ion therapy facility in Korea. In the manufacturing stage, in order to guarantee the hole quality of the holes in the pepper-pot mask, we fabricated two mask using different methods that are made of phosphor bronze by optical lithography process and SUS by laser cutting. After the comparison of each SEM (scanning electron microscope) measurement data, the phosphor bronze mask fabricated by lithography was found to be suitable. The rotation and translation matrices are applied on all images obtained by the camera to mitigate the relative angular misalignment errors between MCP, mirror, and CMOS camera with respect to the mask. By applying the instrument in the NFRI ion source, the four-dimensional phase-space distribution of ion beams is retrieved and compared with the result measured by using a slit-scan method. In this paper, we describe the fabrication process, data analysis method and beam measurement results of the developed emittance meter.

INTRODUCTION

Since the carbon ions in tumor therapy are the elevate relative biological effectiveness (RBE), enhancing the inactivation in the tumor volume while in the entrance channel RBE stays close to one. During the past decade, design and construction of synchrotron-based carbon-ion therapy facilities such as HIMAC, GHMC, SAGA HIMAT, iROCK and HIBMC in Japan, HIT, MIT and GSI in Germany, SPHIC and IMP in China, CNAO in Italy, MedAustron in Austria, and KHIMA in Korea have been carried out all over the world. The biological benefits of carbon ion therapy have been demonstrated in inoperable cases with various types of sarcoma, adenocarcinoma, adenoid cystic carcinoma and malignant melanoma arising from various sites that are well known as photon resistant tumors [1].

The Korea Heavy Ion Medical Accelerator (KHIMA) project was launched in Korea to develop and demonstrate accelerator technologies for a proton and carbon beam based therapy and it is currently under construction. Low-intensity proton and carbon beams with energy in the range of 110 to 430 MeV/u for carbon beams and 60 to 230 MeV for protons, which corresponds to water equilibrium beam range of 3.0 to 27.0 g/cm² are produced by the accelerator for a cancer therapy. The accelerator consists of a low energy beam transport (LEBT) line, radio-frequency quadrupole (RFQ) linear accelerator (linac), interdigital H-mode drift-tube-linac (IH-DTL), medium beam transport (MEBT) line, synchrotron, and high energy beam transport (HEBT) line [2].

* garam@postech.ac.kr

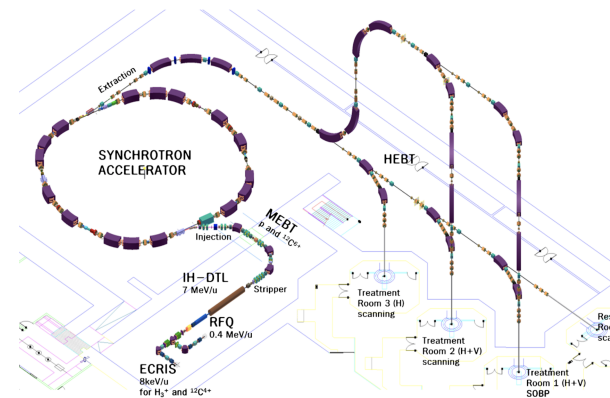


Figure 1: Layout of KHIMA project.

In the low energy beam transport line (LEBT) of the KHIMA accelerator (as shown in Fig. 1), two electron-cyclotron resonance ion sources (ECR-IS) are installed to produce the $^3\text{H}^+$ beam with a nominal current of 328 e μA and $^{12}\text{C}^4+$ beam with a nominal current of 122 e μA respectively, and the energy of ion beams is 8 keV/u that is determined by static extraction voltage [3]. It is important to precisely measure emittances between at the end of LEBT and at the entrance of RFQ, as the mismatching of the beam at this point determines most of the beam transmission ratio, and it affects the number of patients that can be treated. With the conventional diagnostic methodologies such as slit-scanning however it takes a relatively long time and space for accurate characterization of the beam properties at the LEBT section [4]. Therefore, we studied a pepper-pot meter that is a highly influential device to measure the emittance and Twiss parameter within a relatively short space of time.

This paper is structured as follows: First, we show the basic components of the pepper-pot meter, design criteria, and validation of the mask fabrication, which reduces the reconstruction error of emittance analysis of the device. Second, the method for image processing and reconstruction result of 4×4 symmetric moments beam matrix using experimental data with the 24 keV argon beam from ECR-IS are presented. Finally, our conclusion is given in the last section.

DESIGN AND FABRICATION

Design

The pepper-pot emittance meter consists of a mask with a pinhole array for deconvoluting the position and angular information of ion beams using a small opening, a micro-channel plate (MCP) for amplifying the signal intensity, phosphor screen for converting electrons to visible light and optics for measuring the profile. Since the ion beam intensity on the screen is reduced significantly by the mask, the MCP

is required indispensably to improve the signal to noise ratio of the detector. A cross section of the construction drawing of the designed pepper-pot meter is shown in Fig. 2.

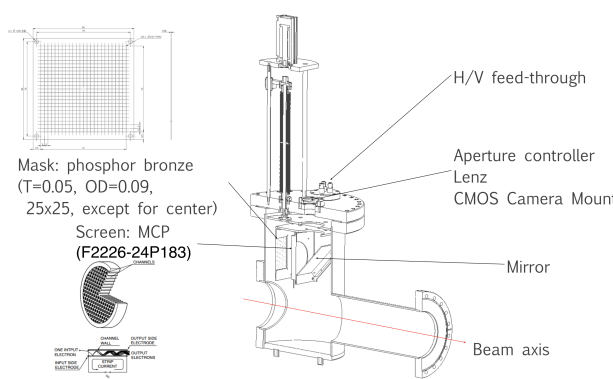


Figure 2: Drawing of pepper-pot emittance meter for KHIMA low energy beamline.

The fundamental principle of the pepper-pot emittance meter is the reconstruction of position and angular distribution of the beam as like the slit-scan method but in a single shot by applying a metallic mask which has equidistant pinholes with the same diameter. When incident ion beams are split into beamlets by the pinholes on the mask, each beamlet creates a spot on the screen downstream from the mask. Consequently, the finite size of each spot is considered to be created by an angular deviation of the beams at the corresponding hole coordinate since the contribution by the hole size is ignorable compared to the influence of the beam angle. This method is deconvoluting the angular information based on the predefined distance between the mask and screen. Therefore, the resolution limit of the beam emittance measurement by using the pepper-pot device is basically determined by the ratio of the distance to pinhole diameter and the precision and deviation of the diameter of pinholes. The distance between the mask and screen was determined to be 5.1 cm to achieve the resolution of better than 3π mm mrad. Main design parameters are listed in Table 1.

Table 1: Main Specifications

Name	Value	Unit
Dimension of mask hole-array	75 × 75	mm
Mask hole configuration	25 × 25-1	–
Mask hole-to-hole distance	3.0	mm
Mask hole diameter	89.9 ± 1.3	μm
Mask to MCP distance	51	mm
MCP active radius	37.5	mm

Mask Fabrication

Two distinct masks were fabricated using substantially different manufacturing techniques with different materials to achieve high manufacturing accuracy and reproducibility

which is a decisive factor for the device. One was made of phosphor bronze by the optical lithography process with a chemical etching and another was made of stainless steel by a laser cutting method. The manufacturing tolerance of hole diameters and distance of both masks is confirmed by an SEM (scanning electron microscope) measurement. The SEM images of two masks are shown Fig. 3.

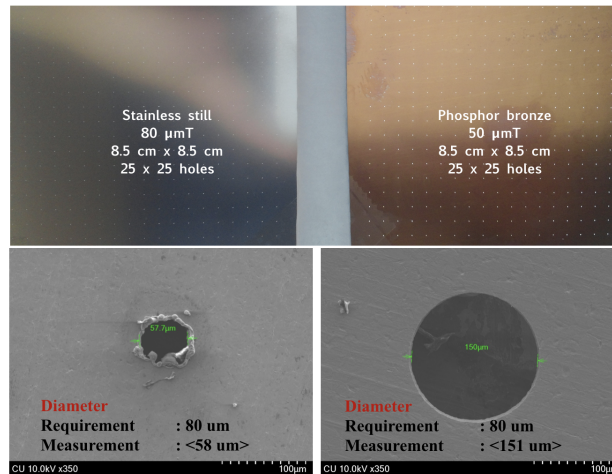


Figure 3: Picture of SEM measurement of two masks; SUS and phosphor bronze.

In the SEM measurement, the irregular burrs formed of the metal by the heat were observed in the SUS mask made by the laser cutting method. These burrs cause the inhomogeneity of the mask hole size explicitly which results in an emittance measurement error due to the incorrectly measured and calculated beam intensity. On the other hand, the phosphor bronze mask made by the optical lithography has the about 30 % bigger holes compared to the original design of the first prototype. Finally, we succeeded to make the hole size similar to design value by controlling etching solution processing time. The distribution of the size of holes was measured to be in the order of $89.9 \pm 1.3 \mu\text{m}$. The result is shown in Fig. 4.

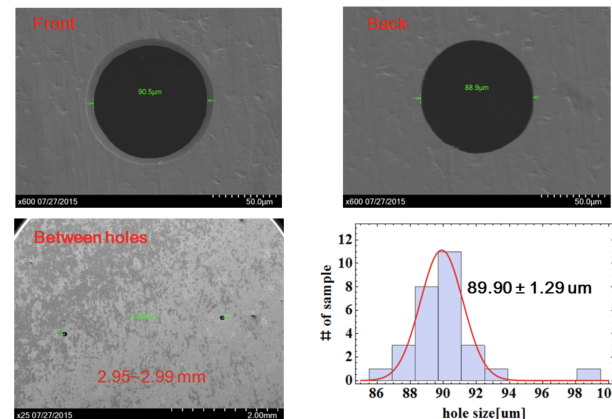


Figure 4: Picture of SEM measurement after fabrication process optimization.

IMAGE PROCESSING AND EXPERIMENT

Image Calibration

Once an image was taken from the camera, before emittance calculation, a correction due to mis-fabrication and mis-alignment was needed. The mask was well aligned related to the vacuum flange, therefore we decided that the misalignment errors came from the wrong position of the mounted camera. To calibrate it, we took a sample image from the camera with the internal light on and with MCP unmounted. Figure 5 shows such errors; left subfigure is a rotation error which is caused by the slightly rotated camera mount on the device. It was simply corrected by applying rotation matrix.

We found that the camera mount position was also shifted from designed location (See Fig. 5-right). The object to image plane was shifted a certain distance proportional to the distance from the CMOS sensor. It means that a shifted beam spot image will be measured even if it is a well centered similar to a tilted beam. Therefore we calculated and applied correction value using the center points of all shown objects with respect to their real distance.

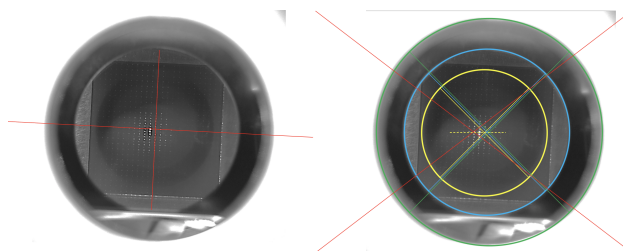


Figure 5: A sample image for the calibration; the left shows the camera rotation error and the right shows the geometrical tilting error due to the shifted view port location.

After the automatic image calibration, the beam calculation was conducted following steps.

1. Background white noise level detection and subtraction
2. Median filtering to reduce impulsive noise due to the dead pixels
3. FFT analysis to divide every pepper-pot beam spot per single grid (See Fig. 6)
4. Four dimensional emittance calculation

Beam Emittance Calculation

The 4×4 symmetric moments beam matrix C can be expressed as [5]

$$C = \begin{bmatrix} \langle xx \rangle & \langle xx' \rangle & \langle xy \rangle & \langle xy' \rangle \\ \langle x'x \rangle & \langle x'x' \rangle & \langle x'y \rangle & \langle x'y' \rangle \\ \langle yx \rangle & \langle yx' \rangle & \langle yy \rangle & \langle yy' \rangle \\ \langle y'x \rangle & \langle y'x' \rangle & \langle y'y \rangle & \langle y'y' \rangle \end{bmatrix} \quad (1)$$

The calculation of the matrix C was possible using the image taken from the pepper-pot emittance meter, because

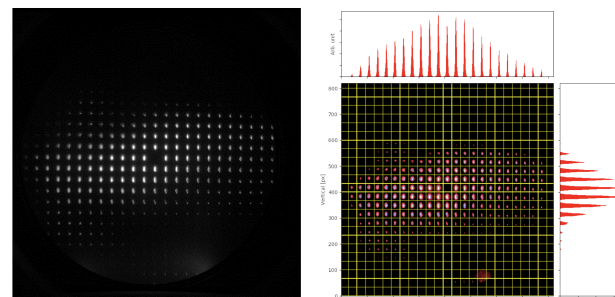


Figure 6: Raw image view(left) and a beam spot partitioning view (right).

every beam spot has its own four independent physical quantities x, x', y, y' . Calculation of such off-diagonal component such as $\langle xy \rangle$ or $\langle x'y \rangle$ is impossible, using the data obtained from the conventional slit scan emittance measurement. Therefore, the pepper-pot device has a big merit to analyze a coupled emittance created by a momentum transfer as well as high speed measurement. Using the matrix C , general beam emittance can be expressed as

$$\epsilon_{ij} = \sqrt{\langle x_i x_j \rangle \langle x'_i x'_j \rangle - \langle x_i x'_j \rangle^2} \quad (2)$$

Emittance measurement was done at NFRI (National Fusion Research Institute) in Korea by using their 28 GHz superconducting ECR ion source. The measured beam was Ar⁸⁺ with current of 70.1 μA and extraction voltage of 24 kV, and the results are shown in Fig. 7 and Fig. 8 overleaf. The 4×4 symmetric moments beam matrix of the measured beam is shown in Eq. (3).

$$C_{\text{measured}} = \begin{bmatrix} 187.68 & 232.86 & 28.80 & 7.92 \\ 232.86 & 313.37 & 39.93 & 16.12 \\ 28.80 & 39.93 & 35.11 & 47.43 \\ 7.92 & 16.12 & 47.43 & 124.86 \end{bmatrix} \quad (3)$$

DISCUSSION

We observed that the light produced by the MCP is reflected partially by surroundings such as the mirror, the mask and vacuum chamber and then it causes strong background on the measured image as shown in Fig. 9. This is challenging to predict the emittance precisely when the background light dilutes the picture of the holes. A vacuum-compatible coating technology is considered for the further upgrade of the device.

CONCLUSION

We developed a pepper-pot emittance meter for the heavy-ion beam emittance measurement. The mask was precisely fabricated through SEM measurement and etching time optimization. After the assembly, the effect of mechanical mis-alignment and mis-fabrication was calibrated by using image processing. Finally we succeeded to measure the emittance at the end of low energy beam transport in NFRI.

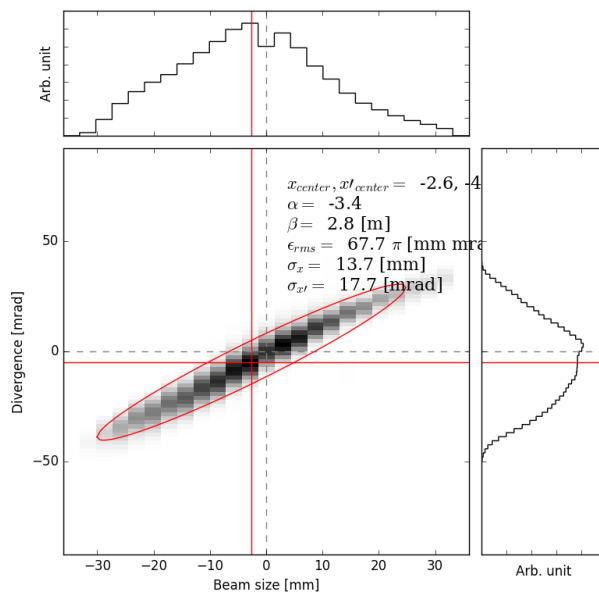


Figure 7: Beam emittance in x - x' phase space.

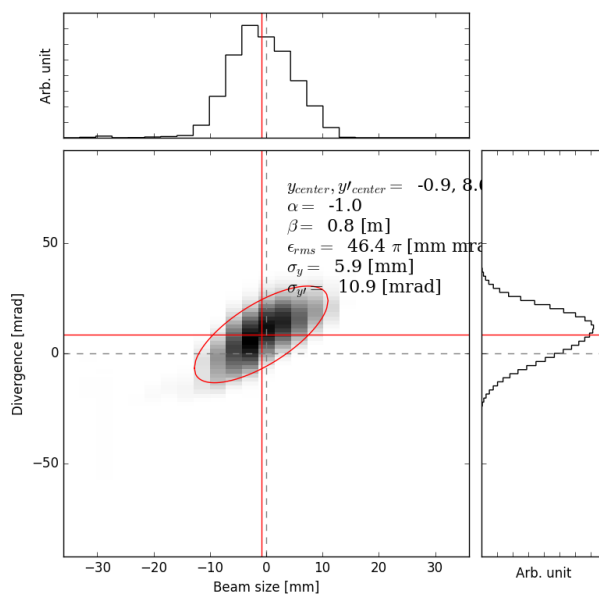


Figure 8: Beam emittance in y - y' phase space.

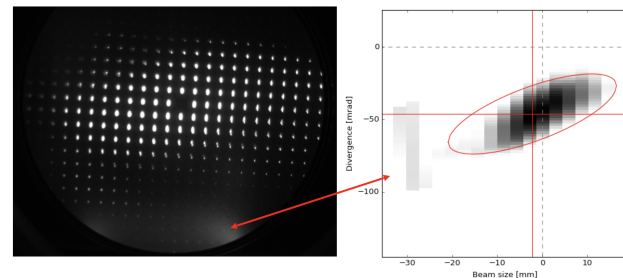


Figure 9: Unwanted MCP background noise and its effect.

ACKNOWLEDGEMENTS

The authors wish to thank their collaborators H.-J. You on National Fusion Research Institute (NFRI) for giving us a chance to commit the beam experiment and Moses Jung on Ulsan National Institute of Science and Technology (UNIST) for valuable discussions about beam calculation.

REFERENCES

- [1] Blakely, E.A., Tobias, C.A., Ngo, F.Q.H. and Curtis, S.B., “Physical and cellular radiobiological properties of heavy ions in relation to cancer therapy application”, in *Pirncello MD, Tobias CA, eds. Biological and Medical Research With Accelerated Heavy Ions at the Bevalac*, CA: LBL-11220; 1980, pp. 73—88.
- [2] G. B. Kim *et al.*, “Korea Heavy Ion Medical Accelerator Project”, in *Proc. 7th Int. Particle Accelerator Conf. (IPAC’16)*, Busan, Korea, May 2016, pp. 4243–4247. doi:10.18429/JACoW-IPAC2016-FRXAA01
- [3] Y. Lee, E.-S. Kim, C. Kim, J. Bahng, Z. Li, G. Hahn, “Start-to-end simulations for beam dynamics in the injector system of the KHIMA heavy ion accelerator”, *Nucl. Instrum. Methods Phys. Res. A*, vol. 528, pp. 7–15, 2017.
- [4] T. K. Yang *et al.*, “Status of Beam Diagnostics at KHIMA Facility”, in *Proc. 4th Int. Beam Instrumentation Conf. (IBIC’15)*, Melbourne, Australia, Sep. 2015, pp. 126–130. doi:10.18429/JACoW-IBIC2015-MOPB038
- [5] K. R. Crandall and D. P., *Los Alamos National Laboratory Report No. LA-UR-97-886*, 1997.